Nano Research
2022, 15(1): 593–602
ISSN 1998-0124 CN 11-5974/O4
https://doi.org/10.1007/s12274-021-3525-6

Research Article

Programmed albumin nanoparticles regulate immunosuppressive pivot to potentiate checkpoint blockade cancer immunotherapy

Liandong Feng[1,2], Li Yang[1], Longjie Li[1], Junying Xiao[1], Nana Bie[3], Chao Xu[1], Jun Zhou[1], Hongmei Liu[1], Lu Gan[3], and Yuzhou Wu[1] (✉)

[1] *Hubei Key Laboratory of Bioinorganic Chemistry and Materia Medica, Hubei Engineering Research Center for Biomaterials and Medical Protective Materials, School of Chemistry and Chemical Engineering, Huazhong University of Science and Technology, Wuhan 430074, China*
[2] *Britton Chance Center for Biomedical Photonics, Wuhan National Laboratory for Optoelectronics-Huazhong University of Science and Technology, Wuhan 430074, China*
[3] *National Engineering Research Center for Nanomedicine, College of Life Science and Technology, Huazhong University of Science and Technology, Wuhan 430074, China*

© Tsinghua University Press and Springer-Verlag GmbH Germany, part of Springer Nature 2021
Received: 1 March 2021 / **Revised:** 14 April 2021 / **Accepted:** 19 April 2021

ABSTRACT

The therapeutic efficacy of programmed cell death protein 1/programmed cell death–ligand 1 (PD-1/PD-L1) blockade immunotherapy is extremely dampened by complex immunosuppressive mechanisms including regulatory T cells (Treg), M2 macrophages (M2), and prostaglandin E2 (PGE2). The pivotal roles of PGE2 have been recognized by directly inactivating CD8+ T cells and indirectly inducing Treg and M2. Therefore, PGE2 abolishment through inactivating cyclooxygenase-2 (COX-2) could be robust to sensitize tumour toward anti-PD-1/PD-L1 immunotherapy, which has gone into clinical trials. However, exploring this promising strategy in nanomedicine to enhance immunotherapy remains unrevealed. The key challenge to synergistically combine COX-2 inhibition and anti-PD-1/PD-L1 lies in the different pharmacokinetic profiles and the spatial obstacles since PD-1/PD-L1 interaction occurs extracellularly and COX-2 locates intracellularly. Thus, the programmed release nanoparticles (termed as Cele-BMS-NPs) are rationally designed, which are composed of pH-sensitive human serum albumin derivative, BMS-202 compound as PD-1/PD-L1 inhibitor, glutathione (GSH)-activatable prodrug of celecoxib (COX-2 inhibitor). The *in vitro* experiments demonstrate that this smart Cele-BMS-NPs could extracellularly release BMS-202 under the acidic tumour microenvironment, and the intracellularly release of celecoxib in response to the elevated GSH concentration inside tumour cells. After systemic administration, the intratumoral infiltration of CD8+ T cells is significantly enhanced and meanwhile immunosuppressive M2, Treg, and PGE2 are reduced, thereby eliciting the anti-tumour immune responses toward low immunogenic tumours and postsurgical tumour recurrences.

KEYWORDS

dual-responsive nanoparticles, programmed release, albumin biopolymer, immunosuppressive environment, immune checkpoint blockade therapy

1 Introduction

The past decade has witnessed exciting advances in the immune checkpoint blockade (ICB) therapy, which leverage the human immune system to eliminate cancer cells. Of particular interest are those systems capable of blockading the programmed cell death protein 1/programmed cell death–ligand 1 (PD-1/PD-L1) or cytotoxic T lymphocyte antigen 4 (CTLA-4) pathway, which sheds light on the treatment of diverse types of cancers, including melanoma, non-small cell lung cancer, renal cell carcinoma, urothelial carcinoma, classical Hodgkin's lymphoma, and even advanced cancers [1–4]. However, the therapeutic efficacy of ICB is still only limited to 5%–30% depending on the tumour types, and it is particularly inefficient for low immunogenic tumours which are surrounded by immunosuppressive environment [5–9]. Several immune evasion mechanisms account for it, including immune suppressive cells such as M2 phenotype macrophages (M2), regulatory T cells (Treg), and immunosuppressive cytokine prostaglandin E2 (PGE2) mainly secreted by cancer cells [10, 11]. Among these immunosuppressive mechanisms, abolishment of PGE2 production by tumour cells is a potential strategy of sensitizing tumours toward anti-PD-1/PD-L1 based immunotherapy through reversing the immunosuppressive environment including M2, Treg, and PGE2 itself [11–16]. Several clinical results have demonstrated that PGE2 abolishment through celecoxib based inactivation of cyclooxygenase-2 (COX-2) could prolong the progression time of patients with metastatic lung cancer and melanoma cancer during anti-PD-1/PD-L1 based immunotherapy [17, 18]. However, small molecule combination of celecoxib and anti-PD-1/PD-L1 antibody also faces several limitations. First, the combination therapy after systemic administration could not achieve optimal synergistic effects due to the different pharmacokinetic profiles. Second, the spatially different locations of molecular targets are another barrier for maximizing the synergistic effects on eliciting anti-cancer immune responses. For example, COX-2 locates in the cytoplasm of cancer cells, while anti-PD-1 based treatment acts on PD-1 protein at the

Address correspondence to wuyuzhou@hust.edu.cn

surface of CD8+ T cells and blocks PD-1/PD-L1 interaction. Thus, the nanomedicines that are able to release anti-PD-1/PD-L1 inhibitors in response to the acidic tumour extracellular environment and help celecoxib to effectively overcome the membrane barrier of tumour cells would be highly attractive to improve ICB efficiency by covering several immune evasion mechanisms [19].

To facilitate the programmed release of drugs, intensive efforts have been devoted to dual stimuli responsive nanoparticles (NPs) [20–24], whose sequential release of drugs can be respectively triggered by dual stimuli [25, 26] or greatly accelerated in the presence of dual stimuli [27–29]. Compared with normal tissues, solid tumours regardless of tumour types are characterized by the acidic extracellular microenvironment (pH 6.5–6.8) [30] and higher intracellular glutathione (GSH) concentration (2–10 mM) [22], which makes it feasible to design the programmed release NPs for transporting PD-1/PD-L1 inhibitors to the extracellular microenvironment and deliver celecoxib into the cytoplasm of tumour cells, respectively. However, the dual drug loaded nanoparticles that meet this site-specific programmed release profiles are rarely reported. To solve this issue, we designed GSH-responsive conjugates of celecoxib to high cationic polymer poly(ethyleneimine), which can promote rapid entry into tumour cells and escape from endosomes/lysosomes to cytoplasm followed by the transformation to active celecoxib [24].

Furthermore, the extracellular release of PD-1/PD-L1 inhibitors is executed by the responsiveness of carrier materials to the acidic extracellular microenvironment of tumours. Based on an "unfolding–refolding" strategy, our group previously developed human serum albumin (HSA) based biopolymers with good biocompatibility, precision structures, and flexible functionalities [31–35]. Theoretically, one molecule of the biopolymer has ~ 128 available reactive amino acid residues to introduce pH-sensitive moieties and ~ 16 free thiols that can be conjugated with polyethylene glycol (PEG) for enhancing *in vivo* stability and blood circulation time. According to the similar strategy we designed pH-sensitive human serum albumin derivatives (psHSA) enriched in a large number of pH-sensitive groups, which can encapsulate PD-1/PD-L1 inhibitors and celecoxib prodrugs into NPs with high stability *in vitro* and *in vivo*, and also high sensitively trigger extracellular release of each drug in responsive to the acidic extracellular microenvironment.

Herein, we developed a programmed release system with pH/GSH dual sensitivity, which synergistically elicits robust anti-tumour immune responses (Fig. 1(a)). These nanoparticles (referring to to Cele-BMS-NPs) are composed of psHSA, small molecular N-{2-[({2-methoxy-6-[(2-methyl[1,1'-biphenyl]-3-yl)methoxy]pyridin-3-yl}methyl)amino]ethyl}acetamide (BMS-202) as PD-1/PD-L1 inhibitors, and the reduction-responsive celecoxib-poly(ethyleneimine) conjugates (termed as PEI-SS-Cele) as GSH activatable COX-2 inhibitor (Fig. 1(b)) [36, 37]. Upon systemic administration, Cele-BMS-NPs are accumulated into tumour via the enhanced permeability and retention (EPR) effect. When exposed to the acidic tumour extracellular environment, psHSA could transform from hydrophobic backbones to hydrophilic ones, which induces the disruption of nanoparticles and results in the release of BMS-202 and PEI-SS-Cele. Cationic PEI-SS-Cele rapidly penetrates cancer cells, escapes from endosomes into cytoplasm where the high level of GSH disrupts disulfide linkages and produces active celecoxib [38, 39]. Then, celecoxib induces COX-2 inactivation and reverses tumour immunosuppressive environment by reducing the levels of PGE2, suppressing Treg and M2 macrophages (Fig. 1). Meanwhile, BMS-202 blocks PD-1/PD-L1 interaction and induces robust anti-tumour immune responses.

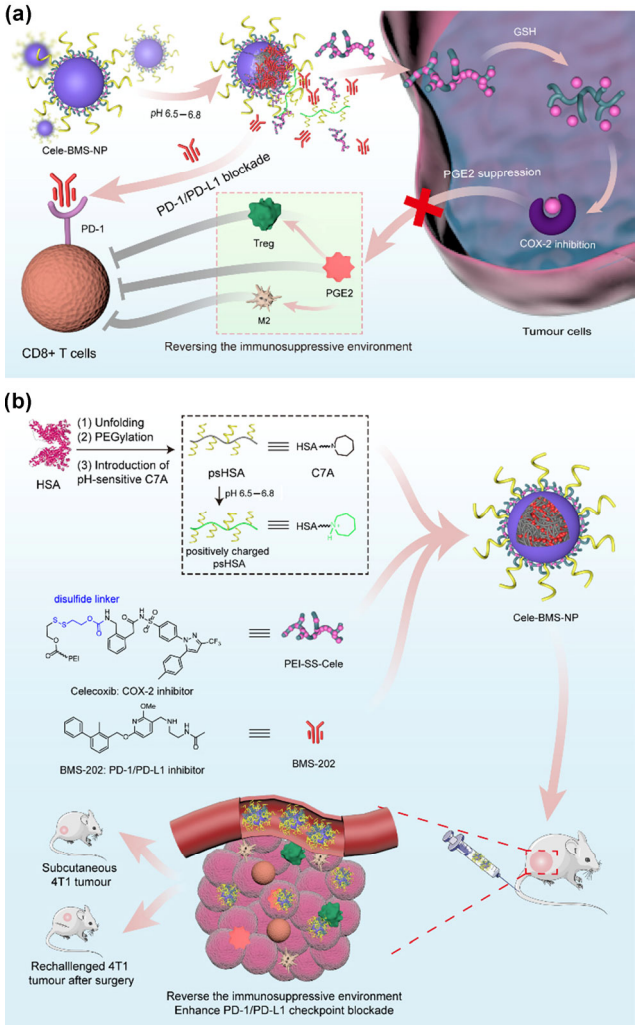

Figure 1 Schematic illustration of the programmed release nanoparticles for the combination of PGE2 suppression and ICB therapy. (a) The proposed mechanisms of improved PD-1/PD-L1 blockade immunotherapy of Cele-BMS-NPs by releasing BMS-202 at the acidic tumour extracellular environment and delivering celecoxib into tumour cells after systemic administration, and thus resulting in reversing tumour immunosuppressive environment involving PGE2, Treg, and M2 macrophages. (b) Fabrication of Cele-BMS-NPs, which were applied to treat subcutaneous 4T1 tumour models and postsurgical 4T1 tumour recurrences.

This strategy appears to be effective in inhibiting tumour growth even for low immunogenic tumours (e.g., 4T1 breast cancer model), and also preventing tumour relapses after surgical resections of primary tumours. Therefore, our strategy shows the promising potentials of improving cancer immunotherapy.

2 Materials and methods

2.1 Materials

Chemicals and reagents: Ethylenediamine, urea, ethylenediamine tetraacetic acid (EDTA), 1-ethyl-(3-dimethylaminopropyl) carbonyldiimide hydrochloride (EDC•HCl), tris(2-carboxyethyl)phosphine hydrochloride (TCEP), succinic anhydride, 2-(azepan-1-yl)ethan-1-amine, 4-dimethylaminopyridine (DMAP), triethylamine (TEA), 1,2-di(pyridin-2-yl)disulfane, 2-mercaptoethanol, 4-nitrophenyl carbonochloridate, 2-(2-(aminomethyl)phenyl)acetic acid, celecoxib, acryloyl chloride, and cyanine5.5 NHS ester (Cy5.5 NHS) were purchased from J&K Chemical (Shanghai, China). mPEG$_{5k}$-maleimide was purchased from Xi'an ruixi Biological Technology Co., Ltd.

(Xi'an, China). Polyethyleneimine with molecular weight of 1,800 Da (PEI_{1800}) was purchased from Shanghai Aladdin Biochemical Technology Co., Ltd. (Shanghai, China). HSA was purchased from Sigma-Aldrich (Shanghai, China). BMS-202 as PD-1/PD-L1 inhibitor was purchased from Topscience Co., Ltd. (Shanghai, China). Hyaluronidase, DNAse I, Dulbecco's modified Eagle's medium (DMEM), Roswell Park Memorial Institute (RPMI) 1640 medium, fetal bovine serum (FBS), and penicillin/streptomycin were purchased from Gibco Inc. (USA). Anti-F4/80-PE (clone: BM8, 0.2 mg·mL^{-1}), anti-CD68-mouse monoclonal antibody (APC) (clone: FA-11, 0.2 mg·mL^{-1}), anti-CD206-fluorescein isothiocyanate (FITC) (clone: C068C2, 0.5 mg·mL^{-1}), anti-CD3-APC (clone: 17A2, 0.2 mg·mL^{-1}), anti-CD4-FITC (clone: GK15, 0.5 mg·mL^{-1}), anti-CD8a-phycoerythrin (PE) (clone: 53–6.7, 0.2 mg·mL^{-1}), anti-Foxp3-PE (clone: MF-14, 0.2 mg·mL^{-1}), and FoxP3 buffer set were all purchased from BioLegend, Inc. (San Diego, USA). PGE2 enzyme linked immunosorbent assay (ELISA) kit were purchased from Abcam. All other chemicals were used as received.

2.2 Cell lines

4T1 cells were purchased from Nanjing KeyGen Biology China (Nanjing, China) and maintained with DMEM supplemented with 10% FBS, penicillin (100 U·mL^{-1}), and streptomycin (100 U·mL^{-1}).

2.3 Animals

Six- to eight-week-age Balb/c female mice were provided by University of Sanxia (Wuhan, China) and used throughout all experiments. All animal procedures were carried out under the guidelines approved by the Institutional Animal Care and Use Committee at Huazhong University of Science and Technology.

2.4 Preparation and characterization of drug loaded nanoparticles

To prepare the dual-drug loaded nanoparticles (Cele-BMS-NPs), the mixture of 121 μL of stock solution of PEI-SS-Cele (equivalent to 3.7 mg·mL^{-1}celecoxib) in N,N-dimethylformamide (DMF), 18 μL of stock solution of BMS-202 (50 mg·mL^{-1}), and 0.46 mL of psHSA solution (32.6 mg·mL^{-1}) in DMF were mixed and left to stand at room temperature for 30 min. The mixture solution and 3.36 μL of 4% glutaraldehyde solution in water were added into 6 mL of phosphate buffered saline (PBS) buffer (pH 7.4) containing 0.5% Pluronic® F-127. After violently stirred overnight, the unencapsulated PEI-SS-Cele, BMS-202, and residual DMF were removed by ultrafiltration at the molecular weight cutoff (MWCO) of 30 kDa. The solution of the Cele-BMS-NPs was finally concentrated to 4.8 mL. The control nanoparticles Cele-NPs and BMS-NPs were prepared according to the same procedure where PEI-SS-Cele and BMS-202 were used instead of the mixture of PEI-SS-Cele and BMS-202. To investigate the cell uptake and *in vivo* distribution of the Cele-BMS-NPs, near infrared fluorescent Cy5.5 labelled Cele-BMS-NPs (Cy5.5-Cele-BMS-NPs) were prepared according to the same procedure by replacing PEI-SS-Cele with Cy5.5-PEI-SS-Cele. The content of Cy5.5 in these nanoparticles was measured by ultraviolet (UV)–visible (vis) absorbance according to stand curve. The amount of celecoxib and BMS-202 was quantified by high performance liquid chromatography (HPLC) assay. The weight ratio of celecoxib to BMS-202 in Cele-BMS-NPs was found to be approximately 6:1. The weight ratio of celecoxib, BMS-202, and Cy5.5 was found to be 6:1:0.8.

To examine pH-responsiveness of nanoparticles, Cele-BMS-NPs were incubated in PBS at pH 6.5 or 7.4, and the particle size and morphology change was then determined by dynamic light scattering (DLS) and transmission electron microscopic (TEM), respectively. The stability of Cele-BMS-NPs was investigated by monitoring the size changes after incubated with PBS, DMEM, and DMEM with 10% FBS with constant shaking at 37 °C for 12, 24, and 48 h.

To investigate the drug release profiles, Cele-BMS-NP solution (0.1 mL) was transferred to dialysis tube (MWCO: 30 kDa) and immersed in 5 mL of PBS buffer (i.e., pH 7.4, 6.5, and 6.5 with 10 mM GSH) with constant shaking at 37 °C. At the predetermined time points, the dialysis solution (0.2 mL) was taken out, and fresh dialysis solution (0.2 mL) was added to measure the concentration of celecoxib and BMS-202 using HPLC assay.

2.5 Cellular uptake

The time-dependent cellular uptake of PEI-SS-Cele was studied by using confocal laser scanning microscopy (CLSM) imaging. 4T1 cells were seeded into a glass bottom dish at a density of 3×10^5 cells per well and cultured overnight. Cy5.5-PEI-SS-Cele (0.5 μM Cy5.5) was added to 4T1 cells and incubated for 15 min, 30 min, and 1 h, respectively. The cells were washed with PBS and stained with Hoechst 33342 for 15 min. The fluorescent images were acquired by CLSM (FV1000, Olympus, Japan). The cellular fluorescent intensity was quantified by using flow cytometric measurement (CytoFLEX, BD Biosciences, Oxford, UK). To investigate the effect of pH on cellular uptake of Cele-BMS-NPs, the cells were treated with Cy5.5-Cele-BMS-NPs (0.5 μM Cy5.5) in medium (i.e., pH 7.4 and 6.5) for 0.5 and 1 h, respectively, and the fluorescent intensity was determined by flow cytometric measurements.

2.6 Inhibition of PGE2 secretion

4T1 cells were seeded into 6-well plate at a density of 2×10^6 cells per well and cultured overnight. PEI-SS-Cele (10 μM celecoxib), Cele-BMS-NPs (10 μM celecoxib), Cele-NPs (10 μM celecoxib), and celecoxib (10 μM) were added to the cells and incubated for 24 h. The cell medium was collected and PGE2 concentration was determined by using a prostaglandin E2 high sensitivity competitive ELISA kit according to the protocol of the manufacturer.

2.7 Biodistribution of Cele-BMS-NPs

To investigate the biodistribution of Cele-BMS-NPs, Balb/c mice were subcutaneously (s.c.) injected with 2×10^6 4T1 cells. When the tumour size reached approximately 200 mm^3, the mice were intravenously (i.v.) injected with Cy5.5-Cele-BMS-NPs (0.25 mg·kg^{-1} Cy5.5; 1.87 mg·kg^{-1} celecoxib; 0.31 mg·kg^{-1} BMS-202). The tumours were imaged by using an *in vivo* imaging system (IVIS) (Xenogen, Alameda, CA) at predetermined time points of 0, 0.5, 1, 2, 4, and 24 h. The mice were sacrificed at 24 h post injection and major organs were collected for analyzing the biodistribution of Cy5.5-Cele-BMS-NPs by determining the fluorescent intensity.

2.8 Anti-tumour effect and postsurgical tumour recurrence prevention

The anti-tumour effect of Cele-BMS-NPs was studied by using Balb/c mice bearing 4T1 breast cancer tumour models. The subcutaneous 4T1 tumour model was established by s.c. injected with 2×10^6 4T1 cells. The mice bearing 4T1 tumours were randomly divided into 5 groups ($n = 6$) when the tumour size reached approximately 200 mm^3. The mice were i.v. injected with PBS, Cele-NPs, BMS-NPs, Cele-BMS-NPs, and celecoxib+BMS-202 at an equal celecoxib dose of 1.87 mg·kg^{-1}

and BMS-202 dose of 0.31 mg·kg^{-1} at day 0, 3, and 6. The tumour volume was determined by a caliper and calculated according to the following formula: width^2 × length × 0.5.

The major organs (heart, liver, spleen, lung, and kidney) were harvested at the end of above anti-tumour experiments, fixed in 10% formalin solution, dehydrated, and subjected to hematoxylin and eosin (H&E) staining.

The prevention of postsurgical tumour recurrences was performed in 4T1 murine breast tumour models. For the primary tumour inoculation, 2 × 10^6 4T1 cells were s.c. injected into the left back of Balb/c mice. When the tumour volume reached approximately 200 mm^3, the primary tumours were resected. Seven days later, the wound healed and the secondary tumours were established by s.c. injecting 2 × 10^6 4T1 cells into the right back of mice, mimicking the postsurgical tumour recurrence models. After 4 days of post injection, the mice were divided into 3 groups (n = 6) and i.v. injected with PBS, Cele-BMS-NPs, and celecoxib+BMS-202 at an equal celecoxib dose of 1.87 mg·kg^{-1} and BMS-202 dose of 0.31 mg·kg^{-1} on day 11, 14, and 17. The tumour recurrences were monitored by measuring the tumour volume.

2.9 Intratumoral infiltration of T cells and M2 macrophages

To investigate the intratumoral infiltration of T cells and M2 macrophages, the subcutaneous tumours were harvested after 3 days of post injection of different formulations and cut into small pieces and immersed in the solution of 0.5 mg·mL^{-1} hyaluronidase, 5 μg·mL^{-1} DNAse I in 1640 medium for 1 h at 37 °C. The single cell suspension solution was obtained by gently pressing the small pieces through cell filters (200 meshes) and stained with fluorescent-labelled antibodies according to the manufacturer's protocols. To analyze M2 macrophages (F4/80+CD68-CD206+), the single cells were stained with anti-F/480-PE, anti-CD68-APC, and anti-CD206-FITC, according to the manufacturer's protocols. For the analysis of CD8+T cells (CD3+CD4-CD8+), the lymphocytes were stained with anti-CD3-APC, anti-CD4-FITC, and anti-CD8-PE, according to the manufacturer's protocols. For detecting Treg cells (CD3+CD4+Foxp3+), the lymphocytes were stained with anti-CD3-APC, anti-CD4-FITC, and anti-Foxp3-PE, according to the manufacturer's protocols. All the samples were determined by using flow cytometric measurements.

2.10 Detection of PGE2 in the serum of mice

Blood was collected from the mice after 3 days of various treatments and centrifuged to harvest the serum. PGE2 concentration was determined by using a PGE2 high sensitivity competitive ELISA kit according to the protocol of the manufacturer.

2.11 Statistical analysis

Results were expressed as the mean ± standard deviation from the data of at least 3 independent experiments. The statistical significance was analyzed by using one-way ANOVA. Statistical significance was set at n.s. (non-significance): $p > 0.05$; *: $p < 0.05$; **: $p < 0.01$; ***: $p < 0.005$.

3 Results and discussion

3.1 Preparation and characterization of Cele-BMS-NPs

HSA, the most abundant protein in blood, was taken as a biocompatible precursor to prepare these nanoparticles [40–43]. Based on an "unfolding–refolding" strategy previously established by us, we could achieve multifunctional HSA derived biopolymers for anticancer drug delivery and bioimaging [31–35]. Herein, we further introduced pH responsive moieties in the HSA derived biopolymers (psHSA) through the following steps: (i) transformation of carboxylic groups on HSA into amino groups; (ii) pegylation of reduced thiol groups in the unfolded HSA backbone with mPEG-maleimide (molecular weight of 5 kDa); (iii) introduction of hexamethyleneimino (C7A) groups to the backbone of HSA via amide coupling, which will get protonated at pH 6.5–6.8 [44–47] endowing the transformation of HSA backbone from hydrophobic to hydrophilic at tumour extracellular environment (Figs. S1 and S2, Table S1 in the Electronic supplementary material (ESM)). The critical micelle concentration (CMC) of the psHSA was found to be 72.4 μg·mL^{-1} (Fig. S3 in the ESM). The responsive pH value of psHSA was determined to be ~ pH 6.75, which indicates the sharp response to the acidic environment around tumour tissue (Fig. S4 in the ESM) [30].

In order to facilitate the intracellular delivery of celecoxib, these drug molecules were conjugated to low molecular weight PEI (average M_W of 1,800 Da) via disulfide bond to prepare the prodrug PEI-SS-Cele (Fig. 2, Figs. S5–S20 in the ESM). Low molecular weight PEI is well known for its rapid uptake by cancer cells due to high cationic charge and extensive use as non-viral gene vectors [38, 39]. Thus, PEI-SS-Cele conjugates could effectively enter into cancer cells through the electrostatic interaction between highly cationic PEI and negatively charged cell membrane followed by endosomes/lysosomes escape via the proton sponge effect, and release celecoxib when exposed to cytoplasmic GSH [36, 37]. The content of celecoxib in PEI-SS-Cele was determined to be ~ 21%wt. The GSH triggered celecoxib release of PEI-SS-Cele was verified by HPLC. After incubation with 10 mM GSH at 37 °C for 12 h, PEI-SS-Cele was degraded with the appearance of the peak attributed to celecoxib (Fig. S21 in the ESM). In contrast, almost no celecoxib was released from PEI-SS-Cele in the absence of GSH. To investigate PEI-SS-Cele uptake, Cy5.5 labelled PEI-SS-Cele (0.5 μM Cy5.5) was incubated with 4T1 tumour cells at different time points. It was found that PEI-SS-Cele rapidly entered into 4T1 cells after 15 min incubation and resulted in a time-dependent uptake as indicated by the fluorescence of Cy5.5 (Fig. 3).

Considering the high cost and immunogenicity of anti-PD-1/PD-L1 antibody, the small-molecule BMS-202 was chosen to block PD-1/PD-L1 interaction [48–50]. Cele-BMS-NPs consisting of psHSA, PEI-SS-Cele, and BMS-202 were prepared by the hydrophobic-hydrophilic phase separation, forming the hydrophobic cores of celecoxib, BMS-202, and HSA backbone and the hydrophilic shells of PEI and PEG (Fig. 1(a)). The mixture of psHSA, celecoxib, and BMS-202 in DMF was dropwise added into the solution of 0.5% Pluoronic F127, which resulted in the self-assembled core–shell nanoparticles. Then, the precursor nanoparticles were cross-linked by glutaraldehyde to enhance the stability. To investigate the sole role of celecoxib or BMS-202 in eliciting anti-tumour immune responses, the nanoparticles loaded with each (abbreviated as Cele-NPs and BMS-NPs, respectively) were also prepared as controls by the similar procedure. Meanwhile, the weight ratio of celecoxib to BMS-202 in the Cele-BMS-NPs was approximately 6:1 as determined by HPLC. TEM images showed the spherical morphology of the Cele-BMS-NPs. The hydrodynamic diameter of 43.5 nm ± 4.0 nm and the zeta potential of 1.72 mV ± 0.74 mV were determined by DLS using ZetasizerTM (Fig. 4(b)). After incubation in PBS at 37 °C for 48 h, Cele-BMS-NPs displayed good stability with slight change in hydrodynamic diameter and slow drug release (Figs. S22 and S23 in the ESM).

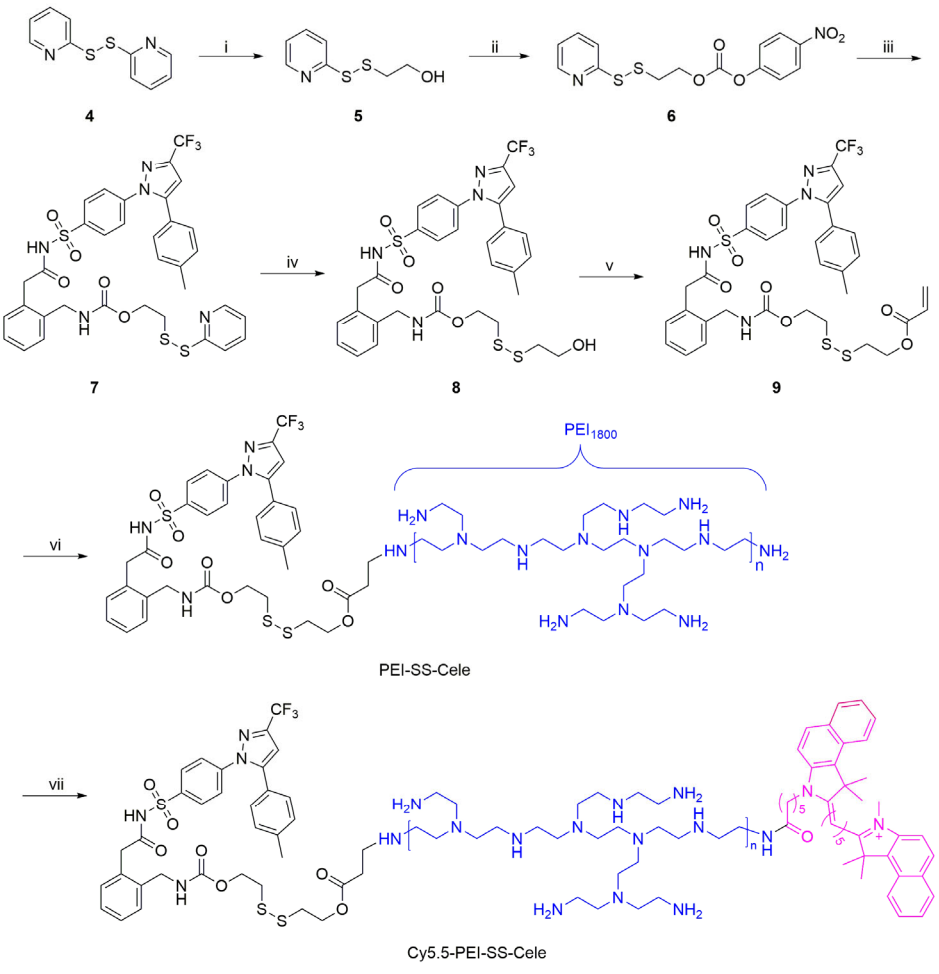

Figure 2 Synthetic route of PEI-SS-Cele and Cy5.5-PEI-SS-Cele. Reaction conditions: (i) acetic acid, MeOH, 24 h, 56.6%; (ii) 4-nitrophenyl chloroformate, TEA, DCM, 73.7%; (iii) 2-(2-(aminomethyl)phenyl)acetic acid, TEA, DCM, 40 °C, 1 h, celecoxib, EDC•HCl, DMAP, DCM, 24 h, 39.6%; (iv) 2-mercaptoethanol, MeOH, overnight, 75%; (v) acryloyl chloride, TEA, DCM, overnight, 28.2%; (vi) PEI_{1800}, TEA, EtOH, 48 h, 56.8%; (vii) Cy5.5-NHS, DMF, overnight, 89%.

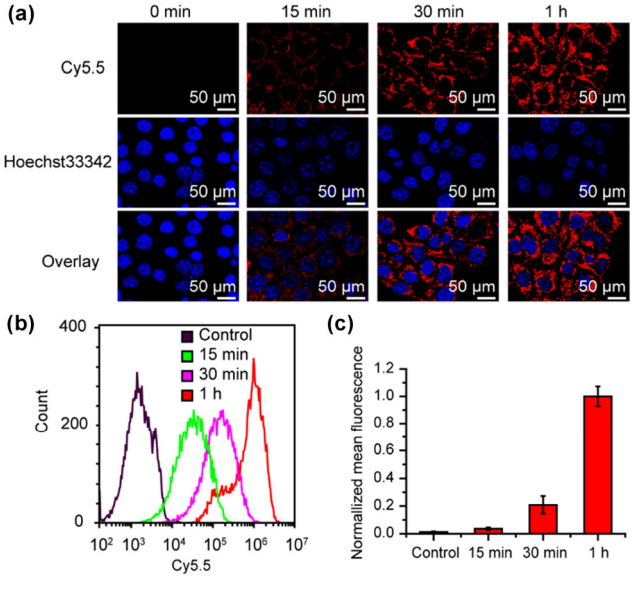

Figure 3 Efficient cellular uptake of PEI-SS-Cele by 4T1 cells. (a) CLSM images of the intracellular uptake of Cy5.5-PEI-SS-Cele in 4T1 cells at different time points. Blue and red represent Hoechst33342 for nucleus staining and Cy5.5 fluorescence for indicating PEI-SS-Cele, respectively. Flow cytometric plot (b) and quantitative analysis of fluorescent intensity (c) of the 4T1 cells treated with Cy5.5-PEI-SS-Cele for the indicated time. Results are expressed as the mean ± standard deviation (n = 3).

3.2 pH- and GSH-responsive property of Cele-BMS-NPs

The pH-responsiveness of Cele-BMS-NPs was also investigated by TEM and DLS. After incubating nanoparticles at pH 7.4 or 6.5 for 24 h, the size of the Cele-BMS-NPs increased from 43.5 nm ± 4.0 nm to 2431 nm ± 271.9 nm due to the protonation of the tertiary amines in the backbone of psHSA (Fig. 4(c)). To validate whether this pH-sensitivity induces the release of BMS-202, we incubated Cele-BMS-NPs in dialysis tube at pH 7.4 or 6.5 and determined the amount of BMS-202 released in the medium at different time points. Over 80% of BMS-202 was released from the Cele-BMS-NPs after incubation at pH 6.5 for 24 h, while less than 30% of BMS-202 was released at pH 7.4 (Fig. 4(d)). These outcomes suggest that the acidic tumour microenvironment (pH 6.5–6.8) can induce faster release of BMS-202 than the neutral environment (pH 7.4) such as blood and normal tissues.

Furthermore, Cele-BMS-NPs exhibited a GSH-dependent release of celecoxib. Minimal amount of celecoxib was detected at pH 7.4 and 6.5 without 10 mM GSH for 24 h. By sharp contrast, Cele-BMS-NPs released more than 80% of celecoxib at pH 6.5 with 10 mM GSH (Fig. 4(d)). Flow cytometric measurements displayed efficient uptake of Cy5.5-Cele-BMS-NPs by 4T1 cells after incubation at pH 7.4 or 6.5 for 0.5 h as indicated by the enhanced fluorescence of Cy5.5 (Fig. 4(e)), which suggested that the disruption of the structures

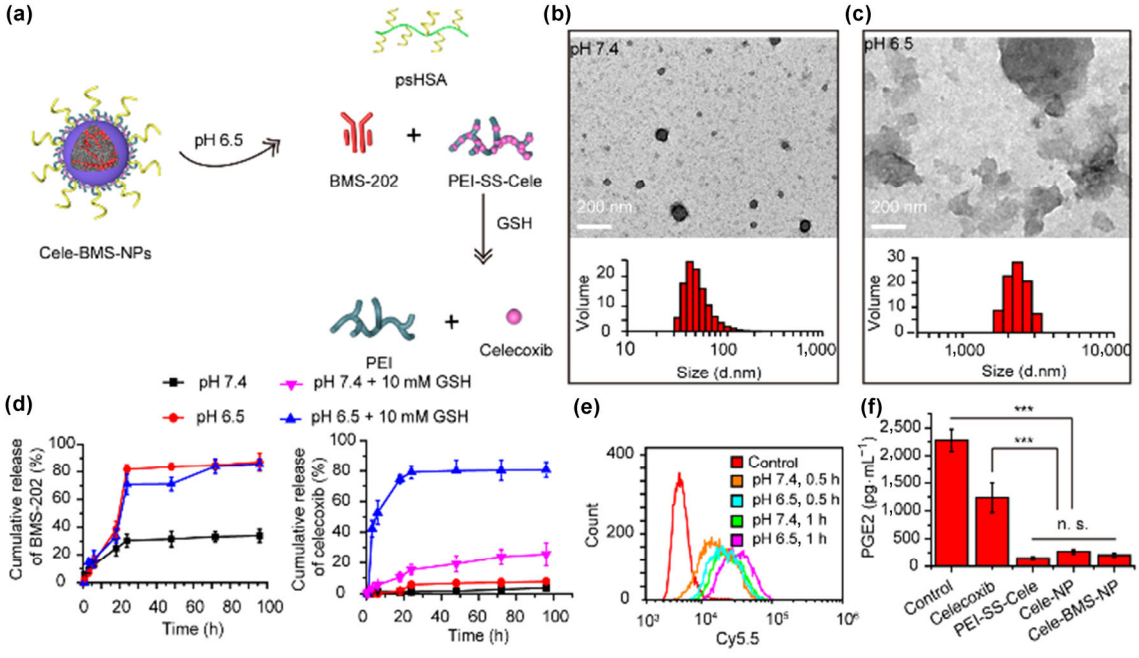

Figure 4 *In vitro* experiment with Cele-BMS-NPs. (a) Schematic illustration for the extracellular release of BMS-202 and the intracellular delivery of celecoxib by Cele-BMS-NPs. (b) and (c) Representative TEM images and hydrodynamic diameter of Cele-BMS-NPs incubated at pH 7.4 or 6.5. (d) BMS-202 and celecoxib release profiles of Cele-BMS-NPs at different conditions. (e) Flow cytometric measurements of the intracellular uptake by 4T1 cells of Cele-BMS-NPs incubated at pH 7.4 or 6.5. (f) PGE2 secretion of control, celecoxib, PEI-SS-Cele, Cele-NPs, and Cele-BMS-NPs by 4T1 cells. Results are expressed as the mean ± standard deviation (n = 3).

of the Cele-BMS-NPs exposed to the acidic environment of pH 6.5 had little disturbance to intracellular delivery of celecoxib. In order to validate the intracellular degradation of PEI-SS-Cele to celecoxib we further tested celecoxib-related COX-2 inhibition properties by measuring PGE2 level secreted by 4T1 cells. Both of Cele-NPs and Cele-BMS-NPs significantly abolished PGE2 production with PGE2 concentration 4.6- and 6.1-fold lower than that in celecoxib group, which is attributed to nanoparticles-mediated efficient cell uptake (Fig. 4(f)). Taken together, Cele-BMS-NPs exhibited programmed spatial release in response to the extracellular stimuli (pH 6.5–6.8) and the intracellular one (GSH).

3.3 Biodistribution of Cele-BMS-NPs *in vivo*

Encouraged by the programmed release of BMS-202 and celecoxib, the tumour accumulation and retention of Cy5.5-Cele-BMS-NPs were examined by *in vivo* fluorescence imaging. Cy5.5 labelled Cele-BMS-NPs (dose of Cy5.5 = 0.25 mg·kg^{-1}, celecoxib = 1.87 mg·kg^{-1}, BMS-202 = 0.31 mg·kg^{-1}) were i.v. injected into 4T1 tumour-bearing Balb/c mice. The Cy5.5 fluorescent signal at tumour sites increased and reached peak intensity at 2 h of postinjection indicating effective tumour accumulation of Cele-BMS-NPs (Fig. 5(a), Fig. S24 in the ESM). Major organs and tumours were collected at 24 h of post injection for *ex vivo* fluorescence imaging. Cy5.5-Cele-BMS-NPs showed the retention at tumour site at 24 h of post injection (Fig. 5(b), Fig. S25 in the ESM).

3.4 Anti-tumour effects and postsurgical tumour recurrence prevention

The *in vivo* anti-tumour efficacy of Cele-BMS-NPs through suppressing PGE2 secretion and prohibiting PD-1/PD-L1 interaction was studied using subcutaneous 4T1 tumour models, which is known to have poor responses to ICB immunotherapy due to the immunosuppression mechanisms [5–7]. Balb/c mice were s.c. injected with 2 × 10^6 4T1 cells per mouse. On day 0, 3, and 6, different formulations were i.v. injected into 4T1 tumour bearing Balb/c mice including PBS, Cele-NPs (celecoxib, 1.87 mg·kg^{-1}), BMS-NPs (BMS-202, 0.31 mg·kg^{-1}), Cele-BMS-NPs (celecoxib, 1.87 mg·kg^{-1}; BMS-202, 0.31 mg·kg^{-1}), and celecoxib+BMS-202 (celecoxib, 1.87 mg·kg^{-1}; BMS-202, 0.31 mg·kg^{-1}). The Cele-BMS-NPs treatment almost completely inhibited the tumour growth, while the single agent-treated groups of Cele-NPs and BMS-NPs slightly delayed the tumour growth in the early days indicating the notable synergistic effect on eliciting anti-tumour immune responses (Fig. 5(c)). In addition, the mice treated with celecoxib+BMS-202 also showed significantly faster speed of the tumour growth than that of the Cele-BMS-NPs group, which is attributed to nanoparticle-enhanced accumulation of drugs at tumuor sites via EPR effect. Furthermore, combination therapy by Cele-BMS-NPs induced negligible weight loss and no histopathological organ damages of the mice at the end of the anti-tumour study suggesting good biocompatibility of Cele-BMS-NPs (Figs. S26–S28 in the ESM).

Resection is the main option for most solid tumours. However, postsurgical tumour relapses remain a great challenge for cancer death, which can be hardly solved by conventional radiotherapy and chemotherapy. A recent study indicates that anti-PD-1 treatment exhibits prevention of postsurgical cancer recurrences [51, 52]. Thus, we wonder if Cele-BMS-NPs inhibit the tumour recurrences after surgery (Fig. 5(d)). The primary tumours were s.c. inoculated with 2 × 10^6 4T1 cells. On day 0, the primary tumours were surgically resected and on day 7 the mice were rechallenged by s.c. injection of 2 × 10^6 4T1 cells, mimicking postsurgical tumour recurrence models. The second tumour growth was monitored in the following 26 days. For the mice treated with PBS, obvious growth of the secondary tumours was observed, while celecoxib+BMS-202 partly delayed the secondary tumour growth in the early days. By sharp contrast, combination treatment with Cele-BMS-NPs almost completely eradicated the secondary tumours, displaying the most notable inhibitory effect on tumour relapses.

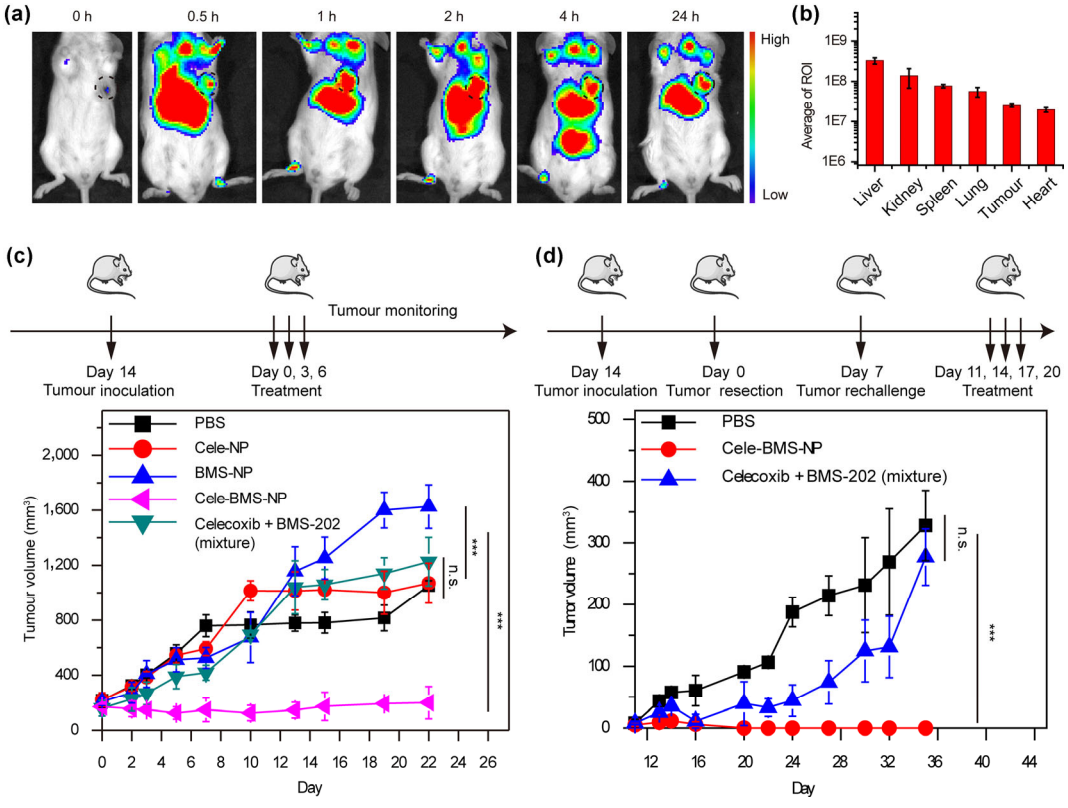

Figure 5 *In vivo* cancer immunotherapy by Cele-BMS-NPs. (a) and (b) Biodistribution of Cy5.5-Cele-BMS-NPs after i.v. administration. (a) Fluorescent images of the subcutaneous 4T1 tumours after i.v. injection of Cy5.5-Cele-BMS-NPs. (b) Organ fluorescence biodistribution of Cy5.5-Cele-BMS-NPs 24 h after i.v. injection. (c) Treatment schedule and the tumour growth curve of subcutaneous 4T1 tumour-bearing mice receiving different formulations, including PBS, Cele-NPs (celecoxib, 1.87 mg·kg^{-1}), BMS-NPs (BMS-202, 0.31 mg·kg^{-1}), Cele-BMS-NPs (celecoxib, 1.87 mg·kg^{-1}; BMS-202, 0.31 mg·kg^{-1}), and celecoxib+BMS-202 (celecoxib, 1.87 mg·kg^{-1}; BMS-202, 0.31 mg·kg^{-1}). Results are expressed as the mean ± standard deviation (n = 6). (d) Treatment schedule and the tumour growth curve of the secondary 4T1 tumours after resection of the primary 4T1 tumours receiving different formulations, including PBS, Cele-BMS-NPs (celecoxib, 1.87 mg·kg^{-1}; BMS-202, 0.31 mg·kg^{-1}), and celecoxib+BMS-202 (celecoxib, 1.87 mg·kg^{-1}; BMS-202, 0.31 mg·kg^{-1}). Results are expressed as the mean ± standard deviation (n = 6).

3.5 The underlying immune mechanisms of cancer immunotherapy

To understand the mechanisms underlying dramatic anti-tumour effect of Cele-BMS-NPs, the tumours were harvested after 3 days of different treatments and analyzed using flow cytometry. Cele-BMS-NPs treatment induced the most notable intratumoral infiltration of CD8+ T cells (5.15% ± 0.58%), which was 1.68-fold that of BMS-NPs, 3.1-fold that of Cele-NPs and untreated group (Figs. 6(a) and 6(d)). However, celecoxib+BMS-202 failed to promote the infiltration of CD8+ T cells to tumours, which might be partly attributed to their differences in pharmacokinetics, biodistribution and cell uptake properties after systemic administration. These results indirectly suggested that BMS-202 blocks PD-1/PD-L1 interaction and resulted in enrichment of CD8+ T cells in tumours, which is crucial executor of anti-PD-1 based immunotherapy.

Next, we investigated the immune suppressive environment of the tumours including Treg cells, M2 macrophages and PGE2 after different treatments for 3 days, which hampered the efficacy of ICB immunotherapy. The percentage of Treg cells in BMS-NPs group remarkably increased to 15.15%, which could partly explain the poor therapeutic efficacy of ICB immunotherapy toward 4T1 breast tumours. In contrast, the Treg infiltration level in Cele-BMS-NPs groups was not significantly increased (Figs. 6(b) and 6(e)). In addition, combination therapy by Cele-BMS-NPs slightly reduced the number of M2 macrophages in comparison to the BMS-NPs group (Figs. 6(c) and 6(f)). Furthermore, both of CD8+ T cells/Treg ratio and CD8+ T cells/M2 ratio were significantly enhanced at tumour sites after Cele-BMS-NPs treatment (Fig. S29 in the ESM). It was shown that Cele-BMS-NPs decreased the PGE2 level in serum to ~ 200 pg·mL^{-1}, while BMS-NPs showed the PGE2 concentration comparable to that in untreated group (Fig. 6(g)). Collectively, the remarkable difference of anti-tumour efficacy between Cele-BMS-NPs and BMS-NPs is mainly attributed to the enhanced tumour infiltration of CD8+ T cells and the significant relievement of tumour immunosuppressive environment including M2, Treg, and PGE2. Our findings showed that PGE2 is a potential target for making 4T1 breast tumours sensitive to anti-PD-1 based immunotherapy.

4 Conclusions

In summary, we have developed a programmed spatial nanoparticles composed of psHSA as encapsulating materials, cationic and reduction-responsive PEI-SS-Cele (celecoxib prodrug, COX-2 inhibitor) and BMS-202 (PD-1/PD-L1 inhibitor) to combine inhibition of PGE2 production and immunotherapy. These nanoparticles can release BMS-202 and PEI-SS-Cele at the tumour extracellular environment due to the protonation of psHSA at pH 6.5–6.8, which induced the disruption of nanoparticles. Meanwhile, PEI-SS-Cele readily enters into tumour cells and escapes from endosomes/lysosomes to cytoplasm via the proton sponge effect, thus subsequently release celecoxib via GSH induced disulfide reduction. The synergistic effect of celecoxib-related inhibition of PGE2 production in the cytoplasm of tumour cells and inhibition of PD-1/PD-L1 interaction occurred on the interface between

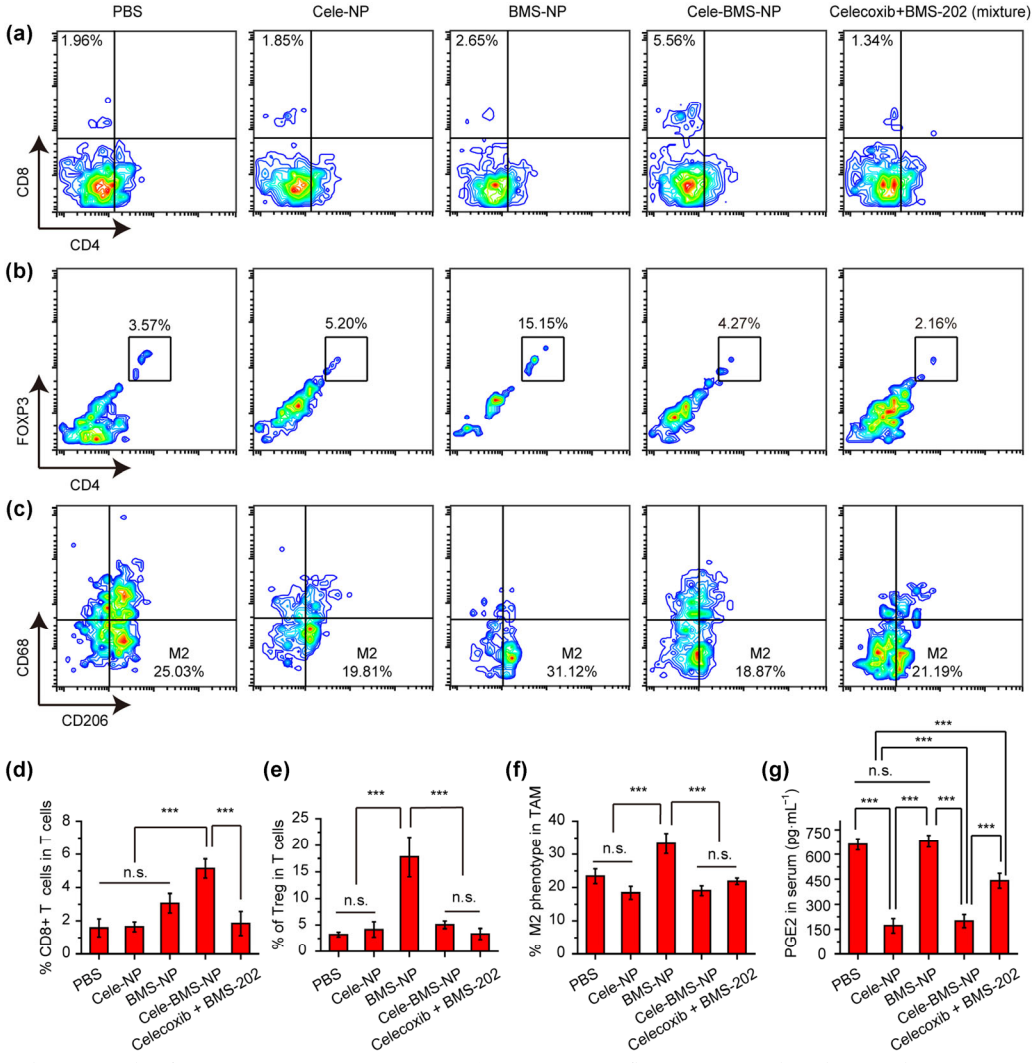

Figure 6 The mechanism study of anti-cancer immune responses. (a) Representative flow cytometry plots showing the percentage of CD8+ T cells (CD4-CD8+) infiltrated into tumour tissues (gated on CD3+ T cells), which were harvested 3 days after the indicated treatment. (b) Representative flow cytometry plots showing the percentage of Tregs (CD4+Foxp3+) infiltrated into tumour tissues (gated on CD3+ T cells), which were harvested 3 days after the indicated treatment. (c) Representative flow cytometry plots showing the percentage of M2 macrophages (CD68-CD206+) infiltrated into tumour tissues (gated on F4/80+), which were harvested 3 days after the indicated treatment. Quantitative analysis of percentage of CD8+ T cells (d), Tregs (e), and M2 macrophages (f). (g) PGE2 level in the sera of mice 3 days after the indicated treatment. Results are expressed as the mean ± standard deviation from the data of at least three independent experiments. The statistical significance was analyzed by using one-way ANOVA. Statistical significance was set at n.s. (non-significance): $p > 0.05$; *: $p < 0.05$; **: $p < 0.01$; ***: $p < 0.005$.

CD8+ T cells and other immune suppressive cells could elicit robust anti-tumour immune responses after systemic administration, achieving inhibition of tumour growth for low immunogenic tumours and prevention of postsurgical tumour recurrences. This strategy overcomes several immunosuppressive mechanisms including PGE2, M2 macrophages, and Treg cells, providing a powerful strategy to improve cancer immunotherapy. Considering the complex immune hijack pathways, this study proposes that the deep understanding of the pivotal therapeutic target in multiple immune evasion mechanisms is highly demanded, which may potentially broaden the application of immune checkpoint blockade therapy to low immunogenic tumours.

Acknowledgements

We acknowledge the financial support from The National Key R&D Program of China (No. 2018YFA0903500), The Postdoctoral Science Fund of China (No. 2017M622429), The National Natural Science Foundation of China (No. 51703073), and The 1000 Young Talent Program of China. We also thank the Analytical and Testing Centre of HUST, Analytical and Testing Centre of School of Chemistry and Chemical Engineering (HUST), and Research Core Facilities for Life Sciences (HUST) for instrument support.

Electronic Supplementary Material: Supplementary material (further details of the annealing and oxidation procedures, STM measurements, AFM imaging and Raman spectroscopy measurements) is available in the online version of this article at https://doi.org/10.1007/s12274-021-3525-6.

References

[1] Couzin-Frankel, J. Cancer immunotherapy. *Science* **2013**, *342*, 1432–1433.

[2] Robert, C.; Schachter, J.; Long, G. V.; Arance, A.; Grob, J. J.; Mortier, L.; Daud, A.; Carlino, M. S.; McNeil, C.; Lotem, M. et al. Pembrolizumab versus ipilimumab in advanced melanoma. *N. Engl. J. Med.* **2015**, *372*, 2521–2532.

[3] Sharma, P.; Allison, J. P. The future of immune checkpoint therapy. *Science* **2015**, *348*, 56–61.

[4] Weber, J. S.; D'Angelo, S. P.; Minor, D.; Hodi, F. S.; Gutzmer, R.;

Neyns, B.; Hoeller, C.; Khushalani, N. I.; Miller, W. H. Jr.; Lao, C. D. et al. Nivolumab versus chemotherapy in patients with advanced melanoma who progressed after anti-CTLA-4 treatment (CheckMate 037): A randomised, controlled, open-label, phase 3 trial. *Lancet Oncol.* **2015**, *16*, 375–384.

[5] Brahmer, J. R.; Tykodi, S. S.; Chow, L. Q. M; Hwu, W. J.; Topalian, S. L.; Hwu, P.; Drake, C. G.; Camacho, L. H.; Kauh, J.; Odunsi, K. et al. Safety and activity of anti-PD-L1 antibody in patients with advanced cancer. *N. Engl. J. Med.* **2012**, *366*, 2455–2465.

[6] Kim, K.; Skora, A. D.; Li, Z. B.; Liu, Q.; Tam, A. J.; Blosser, R. L.; Diaz, L. A. Jr.; Papadopoulos, N.; Kinzler, K. W.; Vogelstein, B. et al. Eradication of metastatic mouse cancers resistant to immune checkpoint blockade by suppression of myeloid-derived cells. *Proc. Natl. Acad. Sci. USA* **2014**, *111*, 11774–11779.

[7] Postow, M. A.; Sidlow, R.; Hellmann, M. D. Immune-related adverse events associated with immune checkpoint blockade. *N. Engl. J. Med.* **2018**, *378*, 158–168.

[8] Lybaert, L.; Vermaelen, K.; De Geest, B. G.; Nuhn, L. Immunoengineering through cancer vaccines—a personalized and multi-step vaccine approach towards precise cancer immunity. *J. Control. Release* **2018**, *289*, 125–145.

[9] Nuhn, L.; De Koker, S.; Van Lint, S.; Zhong, Z. F.; Catani, J. P.; Combes, F.; Deswarte, K.; Li, Y. P.; Lambrecht, B. N.; Lienenklaus, S. et al. Nanoparticle-conjugate TLR7/8 agonist localized immunotherapy provokes safe antitumoral responses. *Adv. Mater.* **2018**, *45*, 1803397.

[10] Butt, A. Q.; Mills, K. H. G. Immunosuppressive networks and checkpoints controlling antitumor immunity and their blockade in the development of cancer immunotherapeutics and vaccines. *Oncogene* **2014**, *33*, 4623–4631.

[11] Adams, J. L.; Smothers, J.; Srinivasan, R.; Hoos, A. Big opportunities for small molecules in immuno-oncology. *Nat. Rev. Drug Discov.* **2015**, *14*, 603–622.

[12] Kryczek, I.; Wei, S.; Zou, L. H.; Zhu, G. F.; Mottram, P.; Xu, H. B.; Chen, L. P.; Zou, W. P. Cutting edge: Induction of B7-H4 on APCs through IL-10: Novel suppressive mode for regulatory T cells. *J. Immunol.* **2006**, *177*, 40–44.

[13] Nakanishi, Y.; Nakatsuji, M.; Seno, H.; Ishizu, S.; Akitake-Kawano, R.; Kanda, K.; Ueo, T.; Komekado, H.; Kawada, M.; Minami, M. et al. COX-2 inhibition alters the phenotype of tumor-associated macrophages from M2 to M1 in $Apc^{Min/+}$ mouse polyps. *Carcinogenesis* **2011**, *32*, 1333–1339.

[14] Ruffell, B.; Affara, N. I.; Coussens, L. M. Differential macrophage programming in the tumor microenvironment. *Trends Immunol.* **2012**, *33*, 119–126.

[15] Noy, R.; Pollard, J. W. Tumor-associated macrophages: From mechanisms to therapy. *Immunity* **2014**, *41*, 49–61.

[16] Mahic, M.; Yaqub, S.; Johansson, C. C.; Taskén, K.; Aandahl, E. M. $FOXP3^+CD4^+CD25^+$ adaptive regulatory T cells express cyclooxygenase-2 and suppress effector T cells by a prostaglandin E_2-dependent mechanism. *J. Immunol.* **2006**, *177*, 246–254.

[17] Wang, S. J.; Khullar, K.; Yegya-Raman, N.; Kim, S.; Silk, A. W.; Malhotra, J.; Gentile, M. A.; Mehnert, J. M.; Jabbour, S. K. Cyclooxygenase inhibitor use during checkpoint blockade immunotherapy and effect on time to progression for metastatic melanoma patients. *J. Clin. Oncol.* **2019**, *37*, e21029.

[18] Wang, S. J.; Khullar, K.; Kim, S.; Yegya-Raman, N.; Malhotra, J.; Groisberg, R.; Crayton, S. H.; Silk, A. W.; Nosher, J. L.; Gentile, M. A. et al. Effect of cyclo-oxygenase inhibitor use during checkpoint blockade immunotherapy in patients with metastatic melanoma and non-small cell lung cancer. *J. ImmunoTher. Cancer* **2020**, *8*, e000889.

[19] Yang, J. X.; Wang, C. H.; Shi, S.; Dong, C. Y. Nanotechnologies for enhancing cancer immunotherapy. *Nano Res.* **2020**, *13*, 2595–2616.

[20] Li, Z. L.; Hu, Y.; Miao, Z. H.; Xu, H.; Li, C. X.; Zhao, Y.; Li, Z.; Chang, M. L.; Ma, Z.; Sun, Y. et al. Dual-stimuli responsive bismuth nanoraspberries for multimodal imaging and combined cancer therapy. *Nano Lett.* **2018**, *18*, 6778–6788.

[21] Rajendrakumar, S. K.; Cherukula, K.; Park, H. J.; Uthaman, S.; Jeong, Y. Y.; Lee, B. I.; Park, I. K. Dual-stimuli-responsive albumin-polyplex nanoassembly for spatially controlled gene release in metastatic breast cancer. *J. Control. Release* **2018**, *276*, 72–83.

[22] Qu, Y.; Chu, B. Y.; Wei, X. W.; Lei, M. Y.; Hu, D. R.; Zha, R. Y.; Zhong, L.; Wang, M. Y.; Wang, F. F.; Qian, Z. Y. Redox/pH dual-stimuli responsive camptothecin prodrug nanogels for "on-demand" drug delivery. *J. Control. Release* **2019**, *296*, 93–106.

[23] Zhang, X. L.; Zhang, C. N.; Cheng, M. B.; Zhang, Y. H.; Wang, W.; Yuan, Z. Dual pH-responsive "charge-reversal like" gold nanoparticles to enhance tumor retention for chemo-radiotherapy. *Nano Res.* **2019**, *12*, 2815–2856.

[24] Zhang, Z. Z.; Wang, Q. X.; Liu, Q.; Zheng, Y. D.; Zheng, C. X.; Yi, K. K.; Zhao, Y.; Gu, Y.; Wang, Y.; Wang, C. et al. Dual-locking nanoparticles disrupt the PD-1/PD-L1 pathway for efficient cancer immunotherapy. *Adv. Mater.* **2019**, *31*, 1905751.

[25] Liu, J. Y.; Liu, W. G.; Weitzhandler, I.; Bhattacharyya, J.; Li, X. H.; Wang, J.; Qi, Y. Z.; Bhattacharjee, S.; Chilkoti, A. Ring-opening polymerization of prodrugs: A versatile approach to prepare well-defined drug-loaded nanoparticles. *Angew. Chem., Int. Ed.* **2015**, *54*, 1002–1006.

[26] Noh, J.; Kwon, B.; Han, E.; Park, M.; Yang, W.; Cho, W.; Yoo, W.; Khang, G.; Lee, D. Amplification of oxidative stress by a dual stimuli-responsive hybrid drug enhances cancer cell death. *Nat. Commun.* **2015**, *6*, 6907.

[27] Feng, L. D.; Wang, Y. Q.; Luo, Z. L.; Huang, Z.; Zhang, Y.; Guo, K.; Ye, D. J. Dual stimuli-responsive nanoparticles for controlled release of anticancer and anti-inflammatory drugs combination. *Chem.–Eur. J.* **2017**, *23*, 9397–9406.

[28] Palanikumar, L.; Jeena, M. T.; Kim, K.; Oh, J. Y.; Kim, C.; Park, M. H.; Ryu, J. H. Spatiotemporally and sequentially-controlled drug release from polymer gatekeeper-hollow silica nanoparticles. *Sci. Rep.* **2017**, *7*, 46540.

[29] Sun, Z. Q.; Liu, G. H.; Hu, J. M.; Liu, S. Y. Photo- and reduction-responsive polymersomes for programmed release of small and macromolecular payloads. *Biomacromolecules* **2018**, *19*, 2071–2081.

[30] Webb, B. A.; Chimenti, M.; Jacobson, M. P.; Barber, D. L. Dysregulated pH: A perfect storm for cancer progression. *Nat. Rev. Cancer* **2011**, *11*, 671–677.

[31] Eisele, K.; Gropeanu, R. A.; Zehendner, C. M.; Rouhanipour, A.; Ramanathan, A.; Mihov, G.; Koynov, K.; Kuhlmann, C. R. W.; Vasudevan, S. G.; Luhmann, H. J. et al. Fine-tuning DNA/albumin polyelectrolyte interactions to produce the efficient transfection agent cBSA-147. *Biomaterials* **2010**, *31*, 8789–8801.

[32] Wu, Y. Z.; Pramanik, G.; Eisele, K.; Weil, T. Convenient approach to polypeptide copolymers derived from native proteins. *Biomacromolecules* **2012**, *13*, 1890–1898.

[33] Wu, Y. Z.; Ihme, S.; Feuring-Buske, M.; Kuan, S. L.; Eisele, K.; Lamla, M.; Wang, Y. R.; Buske, C.; Weil, T. A core–shell albumin copolymer nanotransporter for high capacity loading and two-step release of doxorubicin with enhanced anti-leukemia activity. *Adv. Healthc. Mater.* **2013**, *2*, 884–894.

[34] Meier, C.; Wu, Y. Z.; Pramanik, G.; Weil, T. Self-assembly of high molecular weight polypeptide copolymers studied via diffusion limited aggregation. *Biomacromolecules* **2014**, *15*, 219–227.

[35] Wu, Y. Z.; Ermakova, A.; Liu, W. N.; Pramanik, G.; Vu, T. M.; Kurz, A.; McGuinness, L.; Naydenov, B.; Hafner, S.; Reuter, R. et al. Programmable biopolymers for advancing biomedical applications of fluorescent nanodiamonds. *Adv. Funct. Mater.* **2015**, *25*, 6576–6585.

[36] Alouane, A.; Labruère, R.; Le Saux, T.; Schmidt, F.; Jullien, L. Self-immolative spacers: Kinetic aspects, structure-property relationships, and applications. *Angew. Chem., Int. Ed.* **2015**, *54*, 7492–7509.

[37] Roth, M. E.; Green, O.; Gnaim, S.; Shabat, D. Dendritic, oligomeric, and polymeric self-immolative molecular amplification. *Chem. Rev.* **2016**, *116*, 1309–1352.

[38] Boussif, O.; Zanta, M. A.; Behr, J. P. Optimized galenics improve *in vitro* gene transfer with cationic molecules up to 1000-fold. *Gene Ther.* **1996**, *3*, 1074–1080.

[39] Akinc, A.; Thomas, M.; Klibanov, A. M.; Langer, R. Exploring polyethylenimine-mediated DNA transfection and the proton sponge hypothesis. *J. Gene Med.* **2005**, *7*, 657–663.

[40] Jiang, Y. Y.; Lu, H. X.; Dag, A.; Hart-Smith, G.; Stenzel, M. H. Albumin-polymer conjugate nanoparticles and their interactions with prostate cancer cells in 2D and 3D culture: Comparison between PMMA and PCL. *J. Mater. Chem B* **2016**, *4*, 2017–2027.

[41] Jiang, Y. Y.; Wong, S.; Chen, F.; Chang, T.; Lu, H. X.; Stenzel, M. H. Influencing selectivity to cancer cells with mixed nanoparticles

prepared from albumin-polymer conjugates and block copolymers. *Bioconjug. Chem.* **2017**, *28*, 979–985.

[42] Taguchi, K.; Lu, H. X.; Jiang, Y. Y.; Hung, T. T.; Stenzel, M. H. Safety of nanoparticles based on albumin-polymer conjugates as a carrier of nucleotides for pancreatic cancer therapy. *J. Mater. Chem. B* **2018**, *6*, 6278–6287.

[43] Piloni, A.; Wong, C. K.; Chen, F.; Lord, M.; Walther, A.; Stenzel, M. H. Surface roughness influences the protein corona formation of glycosylated nanoparticles and alter their cellular uptake. *Nanoscale* **2019**, *11*, 23259–23267.

[44] Ko, J. Y.; Park, S.; Lee, H.; Koo, H.; Kim, M. S.; Choi, K.; Kwon, I. C.; Jeong, S. Y.; Kim, K.; Lee, D. S. pH-sensitive nanoflash for tumoral acidic pH imaging in live animals. *Small* **2010**, *6*, 2539–2544.

[45] Zhou, K. J.; Wang, Y. G.; Huang, X. N.; Luby-Phelps, K.; Sumer, B. D.; Gao, J. M. Tunable, ultrasensitive pH-responsive nanoparticles targeting specific endocytic organelles in living cells. *Angew. Chem., Int. Ed.* **2011**, *50*, 6109–6114.

[46] Zhou, K. J.; Liu, H. M.; Zhang, S. R.; Huang, X. N.; Wang, Y. G.; Huang, G.; Sumer, B. D.; Gao, J. M. Multicolored pH-tunable and activatable fluorescence nanoplatform responsive to physiologic pH stimuli. *J. Am. Chem. Soc.* **2012**, *134*, 7803–7811.

[47] Wang, Y. G.; Zhou, K. J.; Huang, G.; Hensley, C.; Huang, X. N.; Ma, X. P.; Zhao, T.; Sumer, B. D.; DeBerardinis, R. J.; Gao, J. M. A nanoparticle-based strategy for the imaging of a broad range of tumours by nonlinear amplification of microenvironment signals. *Nat. Mater.* **2014**, *13*, 204–212.

[48] Guzik, K.; Zak, K. M.; Grudnik, P.; Magiera, K.; Musielak, B.; Törner, R.; Skalniak, L.; Dömling, A.; Dubin, G.; Holak, T. A. Small-molecule inhibitors of the programmed cell death-1/programmed death-ligand 1 (PD-1/PD-L1) interaction via transiently induced protein states and dimerization of PD-L1. *J. Med. Chem.* **2017**, *60*, 5857–5867.

[49] Skalniak, L.; Zak, K. M.; Guzik, K.; Magiera, K.; Musielak, B.; Pachota, M.; Szelazek, B.; Kocik, J.; Grudnik, P.; Tomala, M. et al. Small-molecule inhibitors of PD-1/PD-L1 immune checkpoint alleviate the PD-L1-induced exhaustion of T-cells. *Oncotarget* **2017**, *8*, 72167–72181.

[50] Konstantinidou, M.; Zarganes-Tzitzikas, T.; Magiera-Mularz, K.; Holak, T. A.; Dömling, A. Immune checkpoint PD-1/PD-L1: Is there life beyond antibodies? *Angew. Chem., Int. Ed.* **2018**, *57*, 4840–4848.

[51] Wang, C.; Sun, W. J.; Wright, G.; Wang, A. Z.; Gu, Z. Inflammation-triggered cancer immunotherapy by programmed delivery of CpG and anti-PD1 antibody. *Adv. Mater.* **2016**, *28*, 8912–8920.

[52] Wang, C.; Sun, W. J.; Ye, Y. Q.; Hu, Q. Y.; Bomba, H. N.; Gu, Z. *In situ* activation of platelets with checkpoint inhibitors for post-surgical cancer immunotherapy. *Nat. Biomed. Eng.* **2017**, *1*, 0011.